Applied Catalysis B: Environmental 95 (2010) 446–455

Contents lists available at ScienceDirect

Applied Catalysis B: Environmental

journal homepage: www.elsevier.com/locate/apcatb

Hydrogen production from butane steam reforming over Ni/Ag loaded $MgAl_2O_4$ catalyst

Harim Jeong, Misook Kang *

Department of Chemistry, College of Science, Yeungnam University, Gyeongsan, Gyeongbuk, 712-749, Republic of Korea

ARTICLE INFO

Article history:
Received 11 August 2009
Received in revised form 22 January 2010
Accepted 23 January 2010
Available online 1 February 2010

Keywords:
Hydrogen production
Butane steam-reforming reaction
Ag/Ni-loaded $MgAl_2O_4$
Ni/Ag-loaded $MgAl_2O_4$

ABSTRACT

The intensive coke deposition and reforming at high temperature that occur in the case of the conventional Ni/γ-Al_2O_4 catalyst lead to rapid catalytic deactivation and reduced H_2 production from the hydrocarbon steam-reforming reaction. We used the impregnation approach to synthesize MgO (30 wt%) Al_2O_4 catalysts loaded with bimetallic Ni(15 mol%)/Ag(15 mol%) or Ag/Ni and studied the steam reforming reactions of butane over these catalysts. The Ag-loaded catalyst exhibited significantly higher reforming reactivity compared to the conventional Ni/$MgAl_2O_4$ catalyst. The main products from steam reforming over the Ni/$MgAl_2O_4$ catalyst without the Ag component were H_2, CO, CO_2, and CH_4, with a small amount of $C_2\sim$ hydrocarbons. However, the addition of Ag reduced the degree of carbon deposition and improved the H_2 product selectivity by eliminating the formation of $C_2\sim$ hydrocarbons at temperatures below 750 °C. The catalytic performances differed according to the order in which the added metal precursors were impregnated in each step. The H_2 production was maximized at 68% over Ni(9)/Ag(1)/$MgAl_2O_4$ at 700 °C for 1 h and this high performance continued for up to 53 h.

1. Introduction

Worldwide attention is focusing on renewable energy sources, particularly hydrogen. The catalytic steam reforming of light hydrocarbons to produce hydrogen is of significant industrial importance and is of increasing interest in the context of a hydrogen economy. Research has demonstrated that liquefied petroleum gas (LPG) is a promising fuel for efficient on-board hydrogen generation. LPG offers several advantages over alcoholic compounds such as dimethylether and other hydrocarbons: it is easily handled and transported and the existing infrastructure of city gas is available for its use. Like propane, *n*-butane is a major constituent of LPG and its conversion, in the presence of steam, affects the hydrogen yield according to the following equations [1–3]:

$$n\text{-}C_4H_{10} + 4H_2O = 4CO + 9H_2,\ \Delta H^\circ_{298} = 649.9\ \text{kJ/mol}, \quad (1)$$

$$n\text{-}C_4H_{10} + 8H_2O = 4CO_2 + 13H_2,\ \Delta H^\circ_{298} = 485.3\ \text{kJ/mol}, \quad (2)$$

$$CO + H_2O = CO_2 + H_2,\ \Delta H^\circ_{298} = -41.2\ \text{kJ/mol} \quad (3)$$

Studies on the steam reforming of *n*-butane are scarce in the literature. Commercial steam-reforming processes use Ni-based catalysts because of their acceptably high activity and significantly lower cost in comparison with the alternative precious metal-based catalysts. Recent research has examined the formation of coke over Ni and Ni-Mo catalysts during *n*-butane steam reforming [4–8], the activity/selectivity features of Ni, Pd and Pt catalysts [9–11], and the steam reforming kinetics of various hydrocarbons over Ni catalysts [12,13].

However, nickel-based catalysts are susceptible to deactivation resulting from the deposition of carbon [14–16], even when operating at steam-to-carbon ratios predicted to be thermodynamically outside of the carbon-forming regime. Both reforming and coke deposition are believed to be initiated by the same elementary hydrocarbon activation step. Under steam-reforming conditions, metal surfaces are covered with various CH*x* intermediates. Without a fast steam gasification step to convert these intermediates to CO and H_2, these adsorbed CH*x* species on the Ni surface can undergo further dehydrogenation, polymerization, and rearrangement into highly stable carbon species that not only show low reactivity toward the gasification reaction, but also may dissolve into or encapsulate the Ni particles. In some cases, the dissolution of these carbon species leads to the growth of carbon whiskers that eventually destroy the catalyst and plug the reactor. An especially serious problem in $NiAlO_4$ catalysts is the abrupt catalytic deactivation that occurs at high temperatures above 650 °C, due to the formation of an $NiAlO_3$ spinal structure resulting from the strong sintering between Ni and Al, and this deactivation leads to reactor shutdown and the reversal of the feed gases [17,18].

To overcome these problems, Sato et al. [19] reported that after reductive and oxidative treatment, Ni/MgO and Co/MgO were active for H_2 production, with Ni/MgO exhibiting particularly high

* Corresponding author. Tel.: +82 53 810 2363; fax: +82 53 815 5412.
E-mail address: mskang@ynu.ac.kr (M. Kang).

0926-3373/$ – see front matter © 2010 Elsevier B.V. All rights reserved.
doi:10.1016/j.apcatb.2010.01.026

and stable activity. On Ni/MgO, the extent of catalyst degradation (coking on the catalyst, oxidation of metal, and sintering of metal particles) was found to be minimal, thus confirming the formation of fine Ni^0 particles that interacted strongly with MgO. Aksoylu and co-workers [20] reported that the Pt-Ni catalyst was very prone to catalyst deactivation at low S (steam)/CO ratios accompanied by high C/O_2 ratios, but this problem was not encountered at high S/CO ratios. Additionally, the Pt-Ni catalyst had slightly better activity and selectivity at higher *n*-butane contents, at the expense of becoming more sensitive to coke deposition. However, there are still some problems remaining in terms of the performance, lifetime, and cost of the catalyst.

In this study, Ag was impregnated into Ni-$MgAl_2O_4$, in order to reduce the extent of catalytic deactivation caused by the strong sintering between Ni and Al during *n*-butane steam reforming. The effect of the order of impregnation on the catalytic performance was considered and the physicochemical properties of the catalysts were determined by XRD, H_2-TPR, NH_3-TPD, and XPS analysis. The butane steam reforming reactions were conducted in the temperature range of 300–850 °C at intervals of 50 °C. The effects of the temperature, steam/butane ratio, and residence time on the activity and selectivity of the catalyst were investigated.

2. Experimental

2.1. Preparation of Ag-, Ni-, Ni/Ag-, and Ag/Ni-loaded $MgAl_2O_4$ catalysts

Four catalysts, viz. Ag-, Ni-, Ni/Ag-, and Ag/Ni-loaded $MgAl_2O_4$ batches with various Ag/Ni (wt%) contents, were prepared by the incipient wetness impregnation method as shown in Fig. 1. For Ag/Ni/$MgAl_2O_4$, 1.0 g of γ-Al_2O_3 (Sasol, 250–425 μm, 146 m^2/g) was impregnated with 3.35 g of magnesium chloride ($MgCl_2$ $6H_2O$, 30 wt% MgO, Junsei Co., Japan) in 25 ml of ethanol. The slurry was stirred homogeneously and evaporated below 70 °C for 30 min. $MgAl_2O_4$ was calcined at 500 °C for 1 h in air, followed by impregnation with 1.87 g of nickel nitrate (15 mol%, $Ni(NO_3)_2{\cdot}6H_2O$, Junsei Co. Japan). As an Ag precursor, 0.28 g of silver chloride (15 mol%, AgCl, Junsei Co., Japan) was added by incipient wetness impregnation onto the previously prepared Ni/$MgAl_2O_4$. After being impregnated with Ag, the sample was dried in ambient air, heated in flowing air at a rate of 10 °C/min to 500 °C, and then held isothermally at 500 °C for at least 1 h. The same procedure was used for the preparation of Ni/Ag/$MgAl_2O_4$. The reduction of the four catalysts, Ni(15 mol%)/$MgAl_2O_4$, Ag(15 mol%)/$MgAl_2O_4$, Ag(15 mol%)/Ni(15 mol%)/$MgAl_2O_4$, and Ni(15 mol%)/Ag(15 mol%)/$MgAl_2O_4$, involved reducing with H_2 at 700 °C for 2 h, followed by cooling to room temperature under argon gas.

2.2. Characterizations of Ag-, Ni-, Ni/Ag-, and Ag/Ni-loaded $MgAl_2O_4$ catalysts

The prepared catalysts were identified through powder X-ray diffraction analysis (XRD, model PW 1830 from Philips) with nickel-filtered Cu Kα radiation (40 kV, 100 mA) at 2-theta angles of 5–70°. The scan speed was 10°/min and the time constant was 1 s.

The Brunauer–Emmett–Teller (BET) surface area was measured using a Micrometrics ASAP 2000 instrument. All of the catalysts were degassed before BET surface measurement. The degassing was carried out under vacuum at 120 °C for 1 h, after which the samples were thermally treated at 300 °C for 30 min. The BET surface areas of the catalysts were measured by nitrogen gas adsorption using a continuous flow method with a mixture of nitrogen and helium as the carrier gas.

X-ray photon spectroscopy (XPS) measurements of Mg2p, Ni2p, Ag3d, and Al2p were recorded with an ESCA 2000 (VZ MicroTech, Oxford, UK) system, equipped with a non-monochromatic Al Kα (1486.6 eV) X-ray source. The powders were pelletized at 1.2×10^4 kPa for 1 min and the 1.0-mm pellets were then maintained overnight in a vacuum (1.0×10^{-7} Pa) to remove any water molecules from the surface prior to the measurement. The base pressure of the ESCA system was below 1×10^{-9} Pa. The experiments were conducted with a 200-W source power and an angular acceptance of ±5°. The analyzer axis made an angle of 90° with the specimen surface. A Shirley function was used to subtract the background in the XPS data analysis. The Mg2p, Ni2p, Ag3d, and Al2p XPS signals were fitted using mixed Lorentzian–Gaussian curves.

NH_3-temperature programmed desorption (TPD) measurements were carried out on a conventional TPD system using a Rigaku Thermoflex TG 8110 microthermogravimetric analyzer equipped with a TAS 100 thermal analysis station. The catalysts

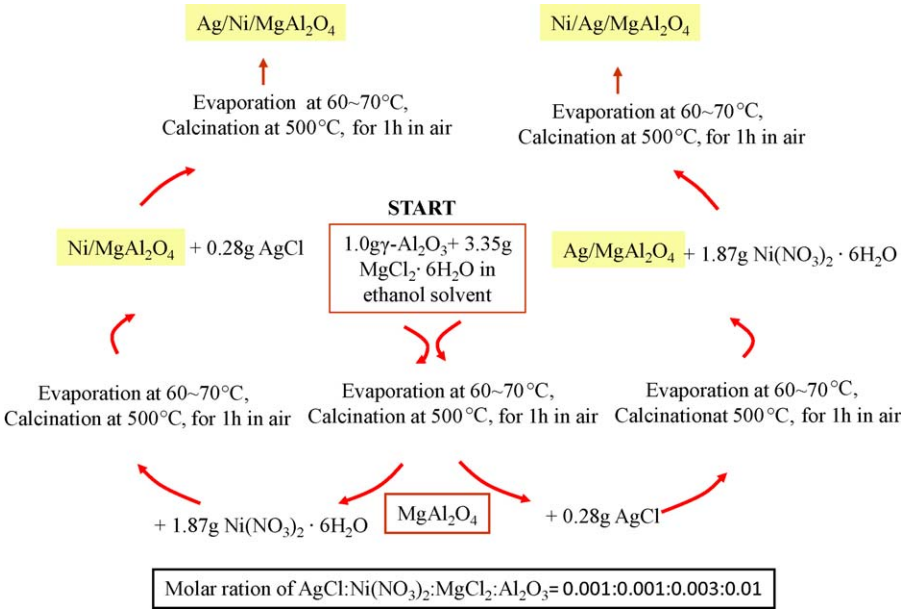

Fig. 1. Preparation of four catalysts, Ag-, Ni-, Ag/Ni- and Ni/Ag-loaded $MgAl_2O_4$ by impregnation method.

were exposed to helium gas at 350 °C for 2 h, in order to remove any water and impurities on the surface. After pre-treatment, the samples were exposed to ammonia for 1 h. Finally, the samples were heated to 650 °C at a programmed heating rate of 10 °C/min. The amount of desorbed gas was continuously monitored by the Thermoflex TG 8110.

H_2-TPR (temperature-programmed reduction) was conducted as follows. About 0.3 g of the catalysts was pre-treated under He flow (30 ml/min) at 700 °C for 2 h and then cooled to room temperature. The analysis was carried out by flowing 30 ml/min of H_2 (10 vol.%)/N_2 and raising the temperature of the catalyst from room temperature to 700 °C at 5 °C/min. The change in the hydrogen concentration was measured with a gas chromatograph (GC series 580, GOW-MAC) equipped with a TCD.

In order to study the formation of carbon species on the catalyst surface, temperature-programmed oxidation (TPO) was performed using a Shimadzu DT-40 thermo-gravimeter by introducing 5% oxygen in helium into the system after purging it with helium. A 20 mg sample was placed in a sample pan and heated from 50 °C to 850 °C at a constant heating rate of 10 °C/min. High-purity air, composed of 21% oxygen and 79% nitrogen, was used as a source of O_2 gas. The gas mixture was diluted to 5% in helium gas and then the diluted gases were flowed at 40 mL/min into the TPO system for the combustion of the carbon accumulated on the catalyst after the reaction. The profiles were obtained in the same manner as that described for TPD, and the coke contents were calculated from the weight loss in the temperature range from 50 °C to 850 °C. α-alumina (20 mg) was used as the reference. The amounts of CO and CO_2 were calibrated by injecting a known amount of the gases from a sample loop into an injection valve in the bypass line.

2.3. Apparatus for butane steam-reforming reaction

The butane steam-reforming activity over the four catalysts, Ag-, Ni-, Ag/Ni-, and Ni/Ag-loaded $MgAl_2O_4$, was measured in the temperature range of 300–850 °C over a the reaction time of 1 h at a steam-to-butane ratio of 1:4 with a GHSV of 5500 h^{-1}: butane gas was directly injected into the reactor, but water was vaporized in a saturator at 100 °C before being injected into the reactor. The amount of steam was adjusted by regulating the temperature, according to the partial pressure equation as follows:

$$\ln P_1/P_2 = -\Delta H/R(1/T_1 - 1/T_2)$$

Here, P_1, P_2, T_1, T_2, ΔH, and R are corresponding to the pressure at 760 mmHg, the pressure on an arbitrary boiling point, the temperature at P_1, the temperature at P_2, the enthalpy, and the gas constant (8.3145 kPa dm^3/mol K), respectively. First, the enthalpy is obtained at all known two-point pressure, and then a pressure (P_1) can be calculated at x mmHg corresponding to the arbitrary volume (or mol) %, and finally the temperature T_1 is determined. Based on this equation, water was introduced into a vaporizer and was vaporized at 60 °C (corresponding to 66% vapor), and the resulting steam was injected into the catalytic reforming reactor using helium gas as a carrier gas. In fact, the C_4H_{10}:H_2O ratio of 1:4 corresponded to flow rates of butane gas and steam of 10 mL/min and 40 mL/min, respectively. The catalyst (0.5 g) was pelletized to 20–25 mesh, packed with a small amount of quartz wool to prevent it from moving in the 10-mm-diameter, fixed-bed metal reactor, and mounted vertically inside the furnace, as shown in Fig. 2. Before testing, the catalysts were reduced in situ for 1 h at 700 °C. Butane diluted with He was supplied from cylinders and the flow rate was adjusted by a flow meter before being mixed in the mixing tank. The amount of water supplied for conversion to vapor was adjusted by a metering valve and introduced into the steam generator along with the mixture. This water was converted to vapor in the vapor generator and then sent to the thermal reactor in the mixed gaseous state. The inlet butane concentration was kept constant at 5 kPa (high purity C_4H_{10}), while the inlet steam concentration was varied depending on the inlet H_2O/butane ratio requirement for each experiment (4.0, 6.5, and 8.0).

After the reactions, the exit gas mixture was transferred via trace-heated lines to the analysis section, which consisted of a carbosphere column equipped with a Donam DS6200 (Donam company, Korea) GC and a mass spectrometer (MS). Gas chromatography was used to investigate the steady state condition experiments, whereas MS, in which the exit gas was sampled by a quartz capillary and differential pumping, was used in the

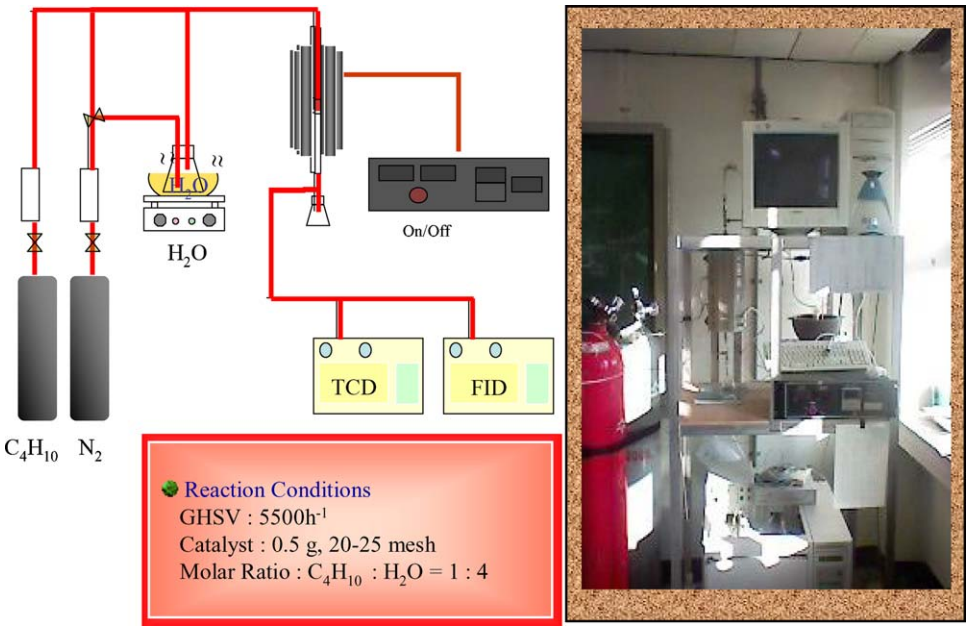

Fig. 2. Apparatus of the catalytic reactor used for butane steam reforming.

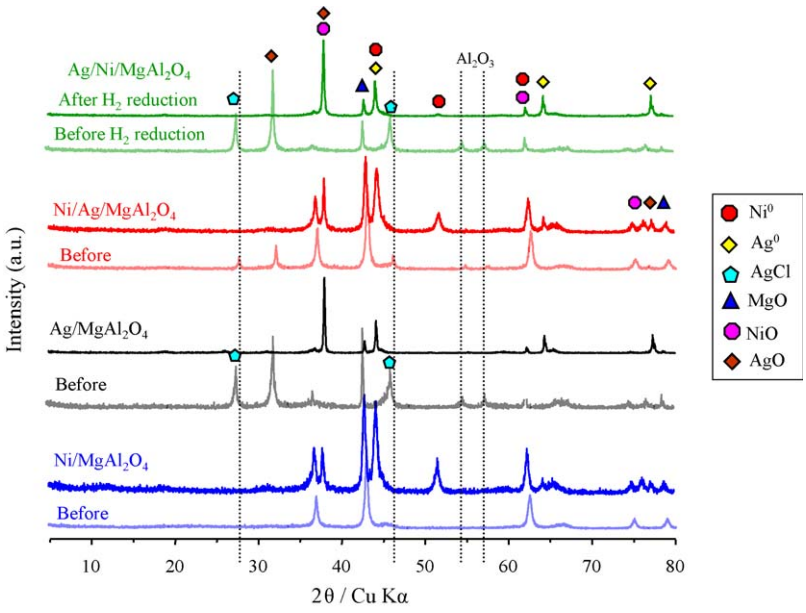

Fig. 3. XRD patterns of four catalysts, Ag-, Ni-, Ag/Ni- and Ni/Ag-loaded $MgAl_2O_4$, before and after H_2 reduction.

transient carbon formation experiment. After the reaction, the catalysts were cooled to room temperature in argon gas and subjected to further characterization. The *n*-C_4H_{10} conversion and H_2, CO and CO_2 selectivities were calculated as described below:

$$n\text{-}C_4H_{10}\ \text{conversion}\ (\%) = [C_{in}\ n\text{-}C_4H_{10} - C_{out}\ n\text{-}C_4H_{10}]/C_{in}\ n\text{-}C_4H_{10} \times 100$$

$$CO_2\ \text{selectivity}\ (\%) = C_{out}CO_2/[C_{out}\ CO_2 + C_{out}CO + C_{out}CH_4 + C_{out}H_2] \times 100$$

$$CH_4\ \text{selectivity}\ (\%) = C_{out}CH_4/[C_{out}\ CO_2 + C_{out}CO + C_{out}CH_4 + C_{out}H_2] \times 100$$

$$CO\ \text{selectivity}\ (\%) = C_{out}CO/[C_{out}\ CO_2 + C_{out}CO + C_{out}CH_4 + C_{out}H_2] \times 100$$

$$H_2\ \text{selectivity}\ (\%) = C_{out}H_2/[C_{out}\ CO_2 + C_{out}CO + C_{out}CH_4 + C_{out}H_2] \times 100$$

3. Results and discussion

3.1. Characteristics of the Ag-, Ni-, Ag/Ni-, and Ni/Ag-loaded $MgAl_2O_4$ catalysts

The Ni(1)-, Ag(1)-, Ni(1)/Ag(1)-, and Ag(1)/Ni(1)-loaded $MgAl_2O_4$ catalysts, both pre-treated and untreated by H_2 gas at 700 °C before the reaction, were characterized by XRD. The XRD patterns are shown in Fig. 3. The special peaks of Al_2O_3, acting in its role of the core metal in the catalysts, were observed at 2-theta angles of 28°, 47°, 55°, and 58° in all of the samples [21], but disappeared during hydrogen reduction, possibly following the complete covering of the catalyst by Ni, Mg, and Ag. Almost no diffraction line of AgO phase at 2-theta angles of around 32° and 79° could be seen in the XRD patterns of the $Ni/MgAl_2O_4$ catalyst. After the H_2 reduction of all of the samples except $Ni/MgAl_2O_4$, AgO was partially reduced to the Ag^0 oxidation state, as shown by the peaks at 2-theta angles of 44° and 65° [22], and Ni^0, which was assigned at 2-theta angles of 43°, 52°, and 62° [23], was also partially observed after H_2 reduction. These results suggested that the oxidation states of the main metal components existed between the oxidized and reduced forms.

Table 1 summarizes the physical properties of the four catalysts. From the energy dispersive X-ray analysis, the loaded metals were different, with the Ni and Ag surface concentrations being relatively higher and lower, respectively. Generally, the surface area shows a strong inverse relation to the particle size; however, this was not the case in our results. The surface areas and pore volumes decreased to a greater extent in the bimetallic-loaded catalysts than in the monometallic-loaded samples. Particularly, these decreases were strengthened by the impregnation of Ag metal, which was attributed to the melting of the Ag particles at high temperature and their subsequent interference with the Ni and Al particle spacing in the bulk material. These symptoms during the butane steam reforming reaction between Ni and Al prevented abrupt sintering.

To determine the relation between the catalytic performance and the Brønsted acidic properties, the NH_3-TPD profiles of the four catalysts were obtained and are shown in Fig. 4. Solid catalytic materials possess many acid sites and certain acidic strengths that are attributed to their high Al contents and tetrahedral Al sites, respectively. The reactions of butane reforming, butane oxidation by oxygen from the injected water, and reduction of carbon oxides in the former and of hydrocarbons by proton ions at the Brønsted acid sites all occur simultaneously. The latter reaction affects the absolute performance of the catalyst. Consequently, the number of

Table 1
Physical properties of four catalysts, Ag-, Ni-, Ag/Ni- and Ni/Ag-loaded $MgAl_2O_4$.

Catalysts	Atomic compositions on the surface of catalysts					BET surface areas (cm^2/g)	Pore volume (cc/g)
	Ni	Ag	Mg	Al	O		
$Ni/MgAl_2O_4$	42.46	–	14.78	7.79	34.99	43.95	0.022
$Ag/MgAl_2O_4$	–	3.31	39.49	14.71	42.48	42.47	0.021
$Ni/Ag/MgAl_2O_4$	48.41	0.45	11.50	8.89	30.73	31.65	0.015
$Ag/Ni/MgAl_2O_4$	7.93	15.03	19.33	12.67	45.01	25.82	0.012

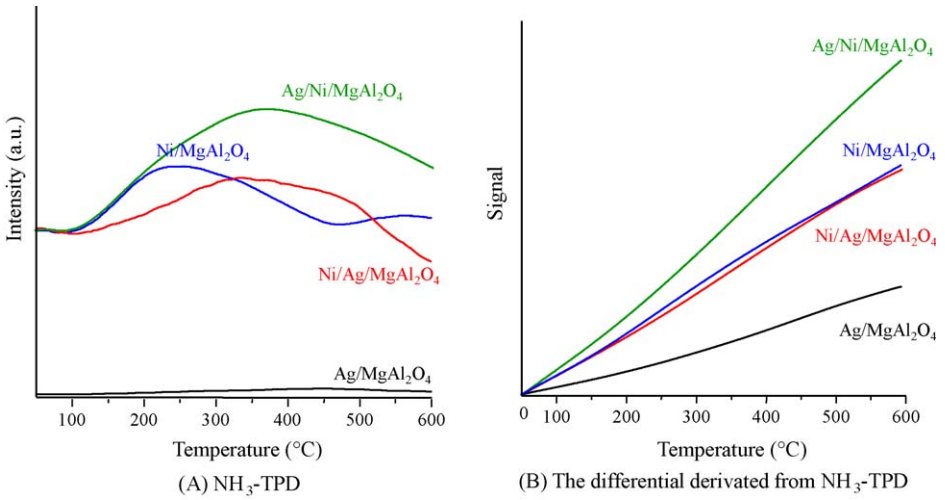

Fig. 4. NH3-TPD curves of four catalysts, Ag-, Ni-, Ag/Ni- and Ni/Ag-loaded $MgAl_2O_4$: (A) NH_3-TPD and (B) the differential derived from NH_3-TPD.

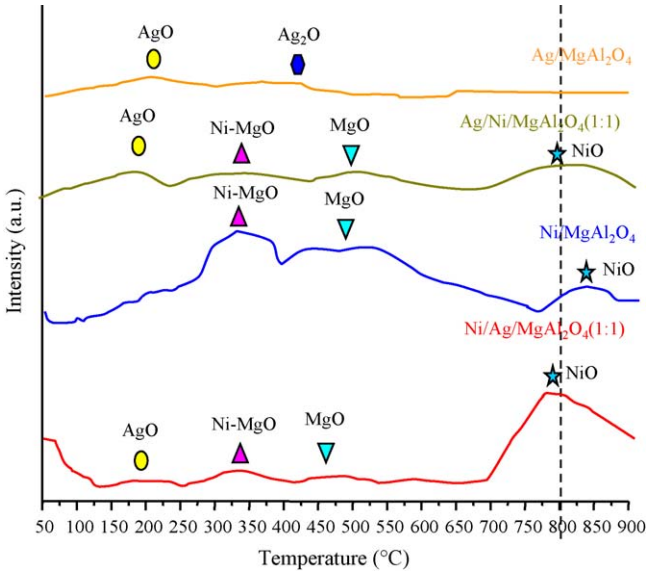

Fig. 5. H_2-TPR curves of four catalysts, Ag-, Ni-, Ag/Ni- and Ni/Ag-loaded $MgAl_2O_4$.

acid sites and their strength are both important. In general, the NH_3-TPD profiles of the four catalysts consist of two peaks: one appears in the low temperature range of 150–250 °C and the other appears in the high temperature range of 400–500 °C. These low and high NH_3-desorption peaks correspond to the weak and strong acid sites, respectively [24]. As shown in Fig. 4, none of the catalysts, except $Ni/MgAl_2O_4$, underwent the separation of the acid sites, and their activation started at 200 °C, while the acidity was the highest at around 350 °C. The significant point was the shift in the acid sites to high temperatures with the addition of the Ag component, and particularly the acidity almost disappeared in the $Ag/MgAl_2O_4$ catalyst. Despite the difference in their acidity, the number of acid sites increased with increasing temperature in all of the catalysts, as shown in Fig. 4B. At this point, we found that the butane reforming reaction was further improved above 300 °C and the activation point was shifted to a higher temperature in the Ag-loaded samples.

The H_2-TPR profiles of the four catalysts are shown in Fig. 5. Four changes corresponding to the reduction of the AgO or Ag_2O, Ni-MgO, MgO, and NiO components are observed in the H_2-TPR profiles. In general, the H_2-TPR results indicate that (1) the peak area corresponds to the hydrogen uptake and (2) the peak at high temperatures corresponds to the catalytic reaction involved in the

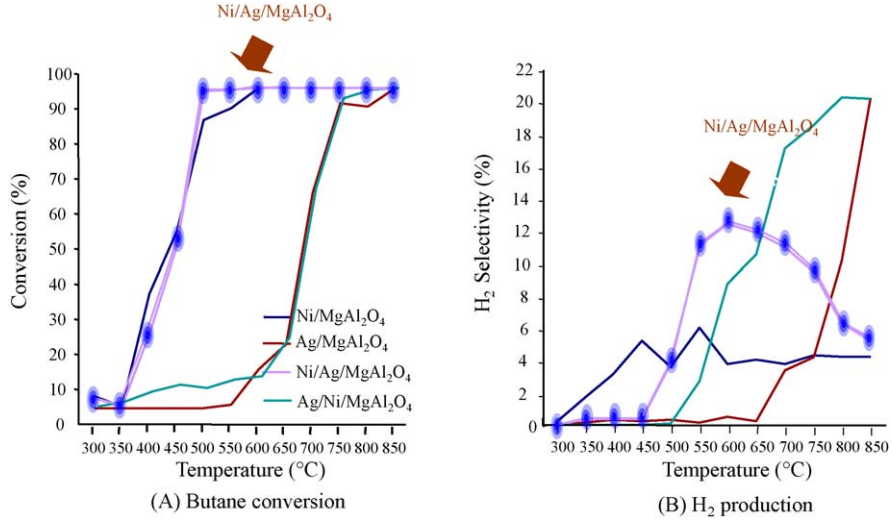

Fig. 6. Butane conversion and H_2 production over four catalysts, Ag-, Ni-, Ag/Ni- and Ni/Ag-loaded $MgAl_2O_4$, according to the reaction temperature: (A) butane conversion and (B) H_2 production.

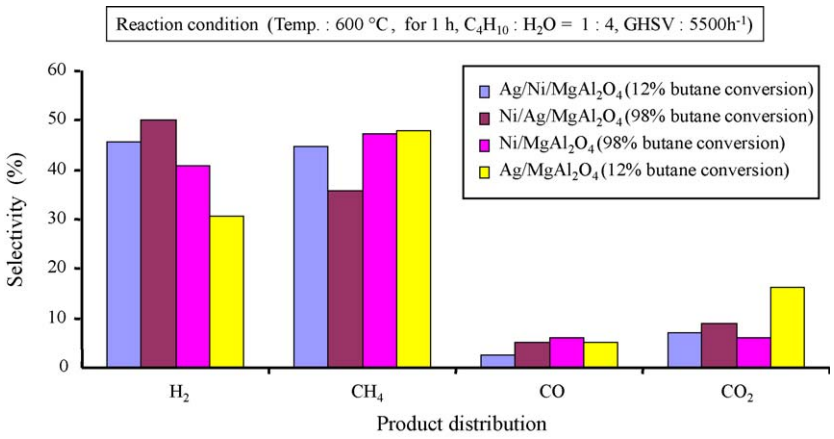

Fig. 7. Production distribution during butane steam reforming over Ni/Ag-loaded $MgAl_2O_4$.

reduction mechanism. In a different result from that of NH_3-TPD in Fig. 4, the reduction peak of NiO was gradually shifted to lower temperatures with increasing Ag addition, and the greatest reduction was observed in the case of Ni/Ag/$MgAl_2O_4$. Additionally, the Ag^{2+} ion was reduced to Ag^0 at a low temperature of 200 °C, while Ag^{1+}, the other silver component was reduced at around 400 °C. Mg and Ni were reduced at 475 °C and 800 °C, respectively, whereas their alloy was reduced at a low temperature of around 325–350 °C.

3.2. Butane steam-reforming reaction over Ni/Ag- or Ag/Ni-loaded $MgAl_2O_4$ catalysts

Butane steam reforming was carried out with 0.5 g of each of the four catalysts, viz. the Ag(1)-, Ni(1)-, Ag(1)/Ni(1)- and Ni(1)/Ag(1)-loaded $MgAl_2O_4$, under the reaction conditions of: temperature = 300–850 °C, GHSV = 5500/h, and H_2O/C_4H_{10} = 4.0. Fig. 6 compares the time-on-stream activity of the four catalysts. In (A), in which only the butane conversion is compared, the conversion over the Ni surface exposed to the catalyst occurred at a relatively low temperature compared with the catalyst-exposed Ag surface. The Ni/Ag/$MgAl_2O_4$ catalytic conversion reached 98% at 450 °C, however, in the most promising result, mostly methane was emitted rather than hydrogen. The proportion of methane emitted was 86%, along with 5% each of CO_2 and CO and less than 2% of hydrogen. This may be caused by methanation on Ni, and details of the methanations of carbon dioxide and carbon monoxide on Ni catalysts can be found in many papers. [25,26] On the other hand, the Ag-loaded catalyst on the external surface provided a significantly higher reforming reactivity compared to the conventional Ni/$MgAl_2O_4$ catalyst. The main products from steam reforming over the Ni/$MgAl_2O_4$ catalyst without the Ag component were H_2, CO, CO_2, and CH_4, with a small amount of C_2∼. However, the addition of Ag reduced the degree of carbon deposition and improved the H_2 product selectivity by eliminating the formation of all C_2∼ type products at temperatures below 750 °C. The catalytic performances differed according to the impregnating order of the added metal precursors in each step, as shown in (B), in which the H_2 production was maximized at 21% over Ag/Ni/$MgAl_2O_4$ at 800 °C. The maximum point of H_2 evolution decreased to 13% at 600 °C over Ni/Ag/$MgAl_2O_4$.

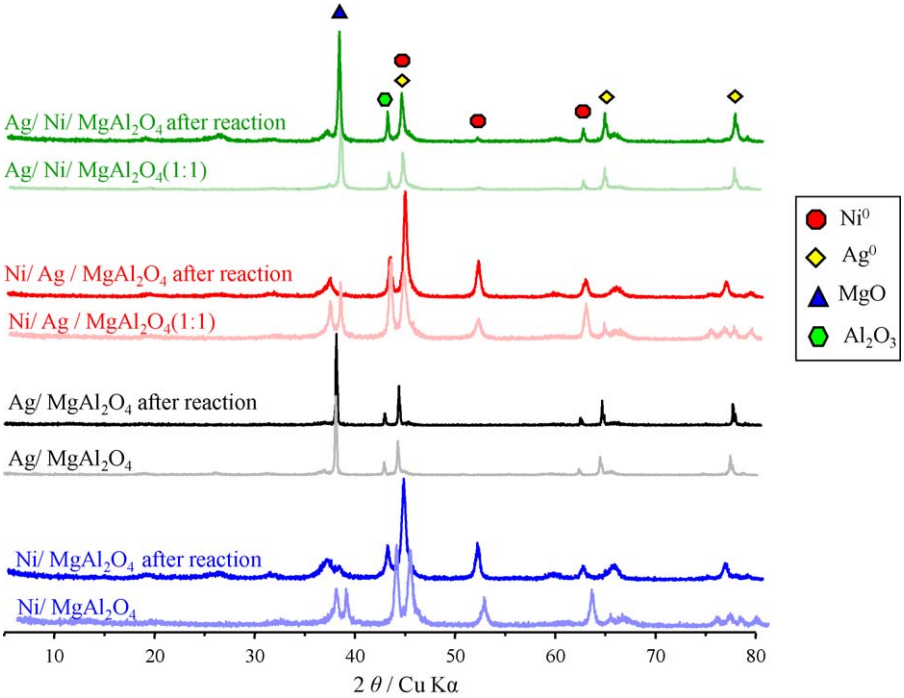

Fig. 8. Comparison of XRD patterns for four catalysts, Ag-, Ni-, Ag/Ni- and Ni/Ag-loaded $MgAl_2O_4$, before and after reaction.

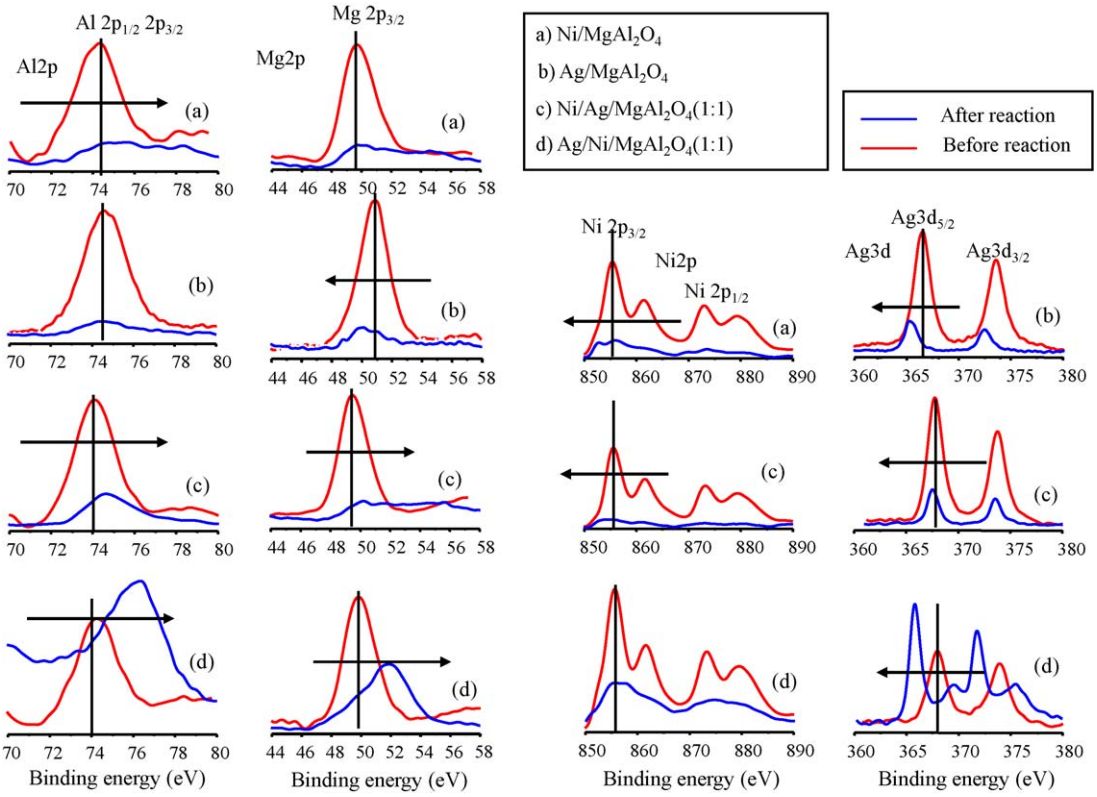

Fig. 9. Comparison of XPS curves for Al2p, Mg2p, Ni2p, and Ag3d orbitals of four catalysts, Ag-, Ni-, Ag/Ni- and Ni/Ag-loaded $MgAl_2O_4$, before and after reaction.

Fig. 7 shows the product distribution obtained from butane steam reforming at 600 °C after 1 h. The product distributions are represented by equivalent to 100% for butane conversion. The reactions were conducted under conditions of C_4H_{10}:H_2O = 1:4, reaction temperature 600 °C, reaction time 1 h, and GHSV 5500 h^{-1}. Four species were present in the product distribution: H_2, CO, CO_2, and CH_4. As shown in this figure, the highest hydrogen selectivity of more than 50% was obtained in the case of Ni(1)/Ag(1)/$MgAl_2O_4$ and decreased in the following order: Ag(1)/Ni(1)/$MgAl_2O_4$ > Ni(1)/$MgAl_2O_4$ > Ag(1)/$MgAl_2O_4$. This result was attributed to the lower sintering between Ni and Al in the Ag-loaded catalysts, which enhanced the hydrogen selectivity during the butane conversion. Unexpectedly, compared with that of the non-Ag catalysts, the CO selectivity of the Ag-loaded catalysts was remarkably decreased to below 5%, whereas their CO_2 production increased. The presence of CO in the fuel cell degrades the active catalyst, due to catalyst poisoning by CO molecules [27]. Therefore, our results demonstrated that the introduction of Ag between Ni and Al had a synergistic effect on the catalytic performance and decreased the sintering phenomenon which leads to catalytic deactivation.

3.3. Characteristics of catalysts after butane reforming

Fig. 8 compares the XRD patterns of the four catalysts after 10 h of reaction at 700 °C. The diffraction lines of the Ni phase shown at 2-theta angles of 38°, 43°, 52°, and 63° show little variation, indicating that the Ni components acted as active sites in the butane steam reforming reaction, as reported in many papers [28,29]. Additionally we found that the peaks of the Ag phases were reduced in oxidation state after the reaction. We, therefore, concluded that the addition of the Ag component helped to retain the stability of the Ni crystallites and avoided their conglomeration in the butane steam reforming reaction, which corresponds to the finding that the Ag/Ni/$MgAl_2O_4$ and Ni/Ag/$MgAl_2O_4$ catalysts have better stability compared with Ni/$MgAl_2O_4$.

Fig. 9 presents the typical survey and high-resolution spectra obtained from the quantitative XPS analysis of the four catalysts. The survey spectra of the particles contained the Al2p, Mg2p, Ni2p, and Ag3d peaks. The Al2p spin-orbital photoelectron, which was assigned to the Al component in γ-Al_2O_3, was located at a binding energy of 74.5 eV for all four samples before the reaction. In general, a large binding energy indicates more oxidized states [30]. After the reaction, the curves were shifted to a higher binding energy, particularly in the spectra of Ni/Ag- and Ag/Ni-loaded $MgAl_2O_4$, although the shift was larger, whereas the change in intensity was not significant, in the latter than in the former. The same phenomenon occurred for Mg2p in two of the samples, Ni/Ag- and Ag/Ni-loaded $MgAl_2O_4$. These results indicate that the Al and Mg ions were oxidized to higher oxidation states after the butane reforming and provide confirmation that the Al and Mg ions were involved in the reduction of butane or other hydrocarbons evolved

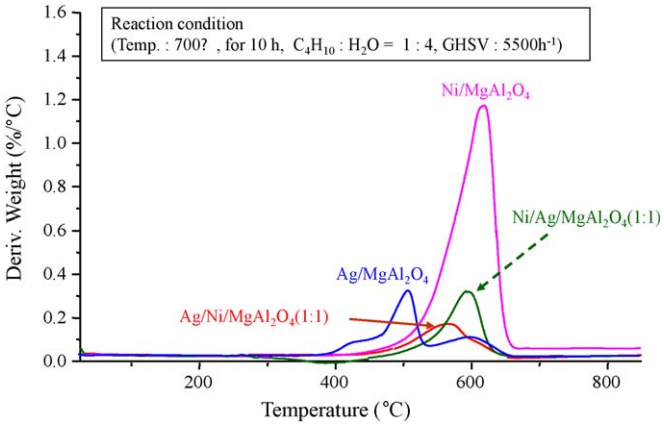

Fig. 10. TPO profiles of four catalysts, Ag-, Ni-, Ag/Ni- and Ni/Ag-loaded $MgAl_2O_4$, after butane steam reforming.

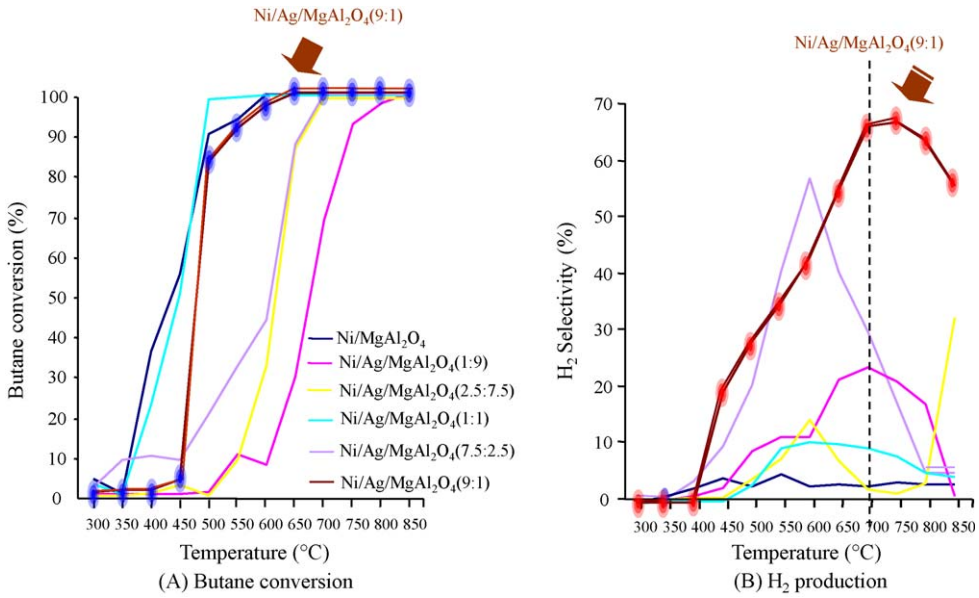

Fig. 11. Butane conversion and H_2 production over $Ni/Ag/MgAl_2O_4$ according to the molar ratio of Ni/Ag: (A) butane conversion and (B) H_2 production.

during the butane reforming reaction to afford the production of H_2 or carbons. On the other hand, the Ag3d region in the spectra of silver oxide was decomposed into two contributions, which were assigned to Ag3d5/2 and Ag3d3/2 at 366.5 eV and 373.5 eV, respectively [31]. In contrast to Al2p and Mg2p, the Ag3d peaks were shifted to a lower binding energy in all of the samples. However, the shift was larger, whereas the change in intensity was not significant, in Ag/Ni-loaded $MgAl_2O_4$ compared to the other samples. Finally, the same phenomenon occurred for Ni2p at a binding energy of 855 eV in the three samples with a Ni component. These results indicate that the Ni and Ag ions were reduced after the butane reforming and, consequently, provide confirmation that the Ni and Ag ions were involved in the oxidation of butane or other hydrocarbons evolved during the butane reforming reaction to afford the production of CO or CO_2 molecules.

To determine the amount of carbon deposited on the catalysts, we carried out TPO measurements, as shown in Fig. 10. The deposited amount and species of carbons are closely related to the catalytic deactivation. Generally, the extent of catalytic deactivation is reduced when a smaller amount of carbon is deposited. Except for $Ni/MgAl_2O_4$, small amounts of carbon were deposited on the Ag-loaded samples. Especially, with the addition of the Ag component to $Ni/MgAl_2O_4$, the amount of carbon deposited remarkably decreased in $Ni/Ag/MgAl_2O_4$ and that deposited over $Ag/Ni/MgAl_2O_4$ was less than 0.2 wt%. On the other hand, when the Ni component was exposed to the outside surface of the $MgAl_2O_4$ samples, the

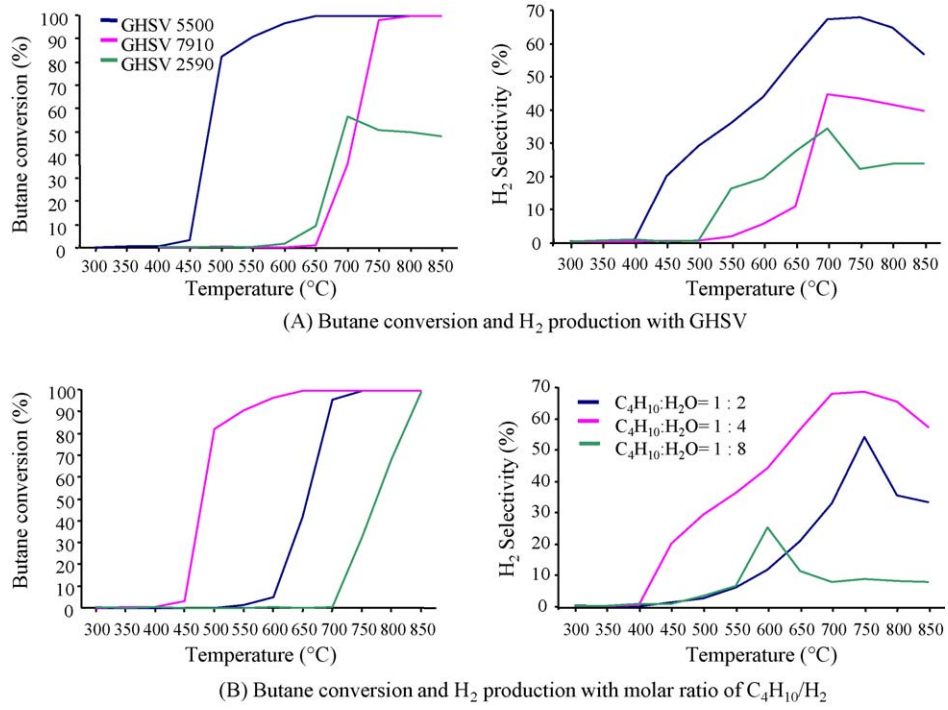

Fig. 12. Butane conversion and H_2 production over $Ni/Ag/MgAl_2O_4$ according to the GHSV and molar ratio of C_4H_{10}/H_2: (A) Variation of butane conversion and H_2 production with GHSV and (B) variation of butane conversion and H_2 production with molar ratio of C_4H_{10}/H_2.

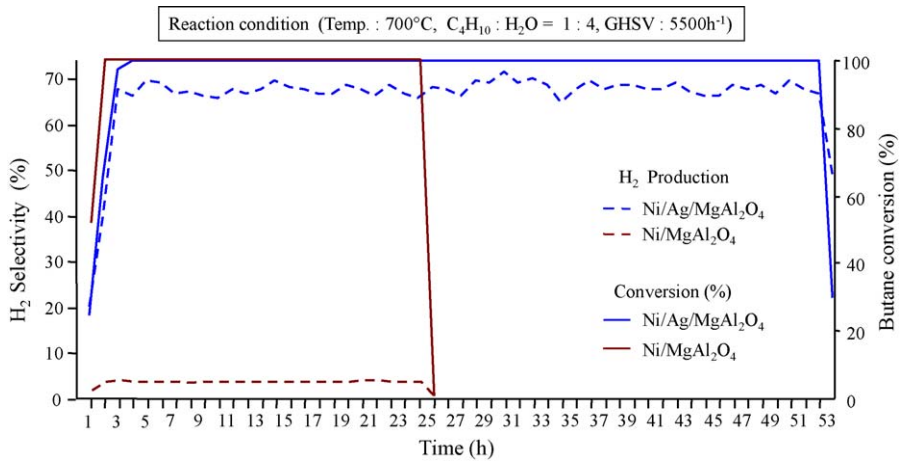

Fig. 13. Test of catalytic deactivation over Ni (9)/Ag (1)/$MgAl_2O_4$.

deposited carbons were oxidized more at high temperatures compared to the sample with the Ag component, indicating the deposition of heavy carbons.

3.4. Optimum conditions for butane reforming

Fig. 11 shows the catalytic performances in the butane reforming reaction over the Ni/Ag/$MgAl_2O_4$ catalysts with various Ni/Ag ratios. Compared to the catalyst without the Ag component, both the butane conversion and H_2 yield improved in almost all of the Ni-loaded samples, particularly the H_2 selectivity, which we attributed to a synergistic effect. As the Ni loading was decreased, the reaction occurred at a higher temperature. Particularly, the butane conversion was above 90% at 550 °C in the case of the catalyst with an Ni:Ag atomic ratio of 9:1, and the butane was converted selectively to hydrogen with a high yield of 68% at

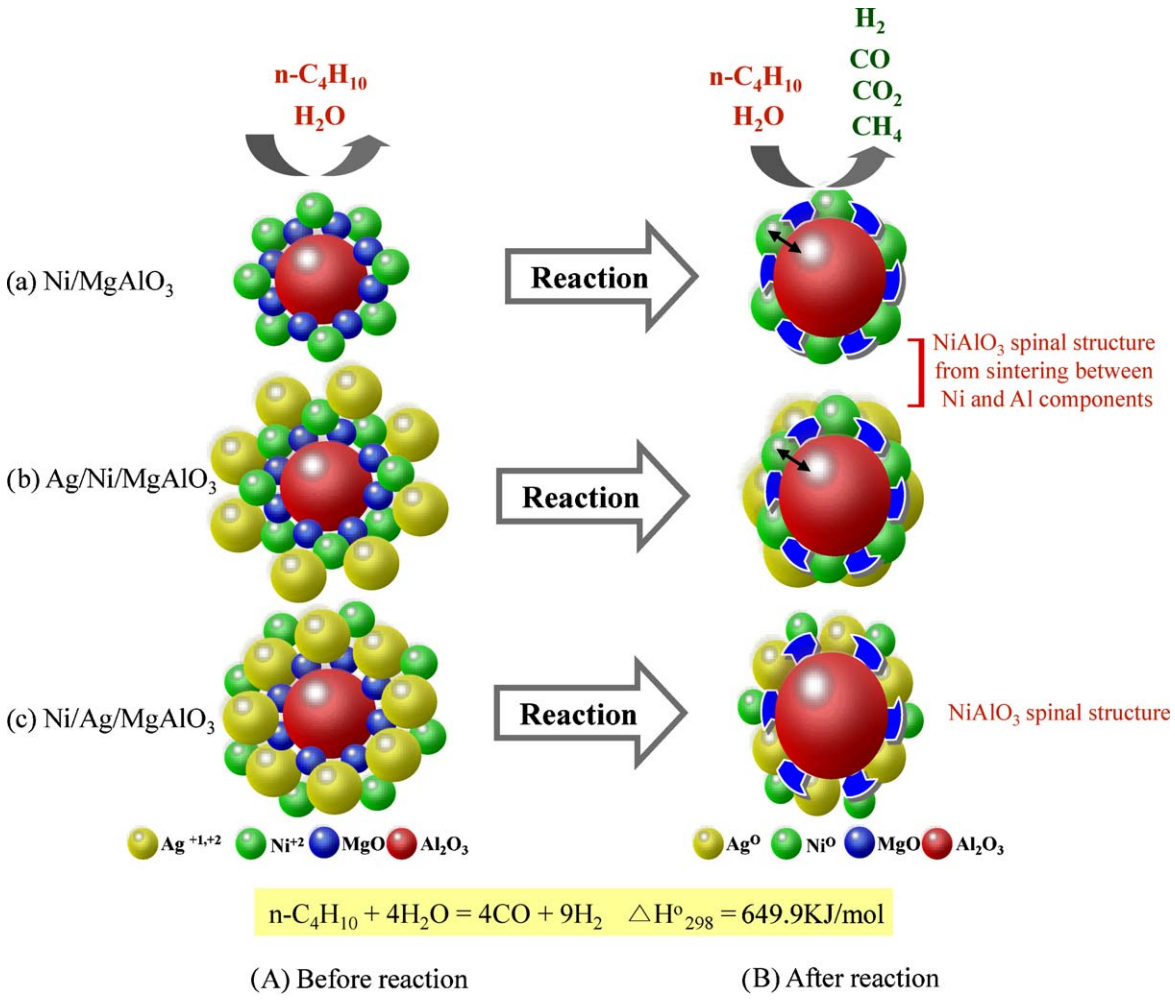

Scheme 1. Expected phase transformation in the butane reforming mechanism before and after butane reforming reaction.

700 °C. These results were significantly different from those reported in other papers. Noticeably, according to the report of Sato et al. [19], the Co/MgO catalyst showed high activity comparable to that of Ni/MgO in authothermal reforming: the n-C_4H_{10} conversion and H_2 yield were 100% and 57%, respectively, at 723 K and SV 67 L/h g after reductive treatment for 0.5 h, but the activity dropped sharply after 15 h. Laosiripojana et al. [32] reported that the main products obtained from steam reforming over CeO_2 were H_2, CO, CO_2, and CH_4 with a small amount of C_2H_4. The dependence of the hydrogen yield on the H_2O/LPG molar ratio, and the H_2 yield was 68% after exposure in the steam reforming condition for 72 h at 900 °C in H_2O/LPG = 7.0. However, the catalysts prepared in this study have two advantages: they are highly active at lower temperatures and exhibit good activity for a long time. This result confirms that the silver ion is as important as the nickel ion in butane reforming.

Fig. 12 shows the optimum reaction conditions for the production of H_2, as determined by the active response: GHSV = 5500/h, butane/H_2O mole ratio = 1/4, and reaction temperature = 700 °C. Additionally, the H_2 production slightly decreased with increasing number of H_2O molecules, resulting in strong sintering between the component metals. Finally, the catalytic deactivation was tested for the two types of catalyst, Ni/Ag/$MgAl_2O_4$ and Ni/$MgAl_2O_4$, and the results are shown in Fig. 13. In a dramatic result, the difference in H_2 production between these two catalysts reached 0.75 mol depending on the presence or absence of Ag. The result is very significant compared with the H_2 production previously reported [33–35]. The catalyst lifetime was greatly improved in Ni/Ag/$MgAl_2O_4$ compared to that of the catalyst without Ag. The catalytic deactivation progressed remarkably after 25 h over Ni/$MgAl_2O_4$, and both the H_2 production and butane reforming rapidly decreased. The rapid deactivation over Ni/$MgAl_2O_4$ indicated that the initial catalyst deactivation may result from a combination of steam-induced nickel sintering and carbon deposition. However, the apparent deactivation rate was far lower for the Ag-promoted catalyst and its higher butane conversion of 100% and H_2 yield of 0.8 mol continued for up to 53 h. Thus, the improved stability at the slower deactivation rate achieved with the Ni/Ag sample could not be unequivocally attributed to carbon formation.

The two key findings of this study are that the difference in H_2 production between the catalysts peaked at 0.75 mol depending on the presence or absence of Ag, and that the catalytic deactivation was retarded by the addition of Ag. On the basis of the performance results and a variety of physical measurements, we proposed Scheme 1 for the catalytic phase change and butane reforming mechanism. During butane reforming, the Ag and Ni components played a role in the oxidation of the feed gases. Butane or other hydrocarbons were produced by reduction. The simultaneous addition of Ag/Ni may have depressed the $NiAlO_3$ spinal structure and induced catalytic deactivation, due to their strong sintering. Consequently, their synergistic effect produced high butane reforming and H_2 production over Ni/Ag/$MgAl_2O_4$.

4. Conclusion

In the present work, Ag was added between Ni and Al in an attempt to decrease the catalytic deactivation induced by the strong sintering between them during n-butane steam reforming, while simultaneously improving the catalytic activity. First, we confirmed that the catalytic performances differed according to the order in which the metal precursors were added. From the XRD analysis before and after the reaction, we also concluded that the addition of the Ag component helped to retain the stability of the Ni crystallites and prevent their conglomeration in butane steam reforming. The H_2 production and butane conversion reached 68% and 100%, respectively, over Ni(9)/Ag(1)/$MgAl_2O_4$ and this high performance continued for up to 53 h. The optimum operation conditions, viz. a reaction temperature of 700 °C, gas hourly space velocity (GHSV) of 5500 h^{-1}, and feed ratio of n-butane: H_2O of 1:4, were identified by a parametric study.

References

[1] Y.-H. Chin, D.L. King, S.-H. Roh, Y. Wang, S.M. Heald, J. Catal. 244 (2006) 153.
[2] A.K. Avcı, Z.I. Önsan, D.L. Trimm, Appl. Catal. A 216 (2001) 243.
[3] A.K. Avcı, D.L. Trimm, A.E. Aksoylu, Z.I. Önsan, Appl. Catal. A 258 (2004) 235.
[4] A.K. Avcı, D.L. Trimm, A.E. Aksoylu, Z.I. Önsan, Catal. Lett. 88 (2003) 17.
[5] T. Borowiecki, W. Grzegorczyk, A. Denis, A. Golebiowski, Catal. Lett. 79 (2002) 119.
[6] L. Kepinski, B. Stasinska, T. Borowiecki, Carbon 38 (2000) 1845.
[7] J. Sehested, Catal. Today 111 (2006) 103.
[8] L.M. Madeira, M.F. Portela, C. Mazzocchia, Catal. Rev. 46 (2004) 53.
[9] X. Wang, R.J. Gorte, Catal. Lett. 73 (2001) 15.
[10] X. Wang, R.J. Gorte, Appl. Catal. A 224 (2002) 209.
[11] R.V. Malyala, C.V. Rode, M. Arai, S.G. Hegde, R.V. Chaudhari, Appl. Catal A 193 (2000) 71.
[12] J.R. Rostrup-Nielsen, J.R. Anderson, M. Boudart (Eds.), Catalysis, Science and Technology, vol. 5, Springer, Berlin, 1984, p. 3.
[13] M.H. Kim, E.K. Lee, J.H. Jun, S.J. Kong, G.Y. Han, B.K. Lee, T.-J. Lee, K.J. Yoon, Int. J. Hydrogen Energy 29 (2004) 187.
[14] J. Xu, L. Chen, K.F. Tana, A. Borgna, Mark Saeys, J. Catal. 261 (2009) 158.
[15] V.C.H. Kroll, H.M. Swaan, C. Mirodatos, J. Catal. 161 (1996) 409.
[16] H.M. Swaan, V.C.H. Kroll, G.A. Martin, C. Mirodatos, Catal. Today 21 (1994) 571.
[17] J.R. Rostrup-Nielsen, J.R. Anderson, M. Boudart (Eds.), Catalysis, Science, and Technology, vol. 5, Springer-Verlag, Berlin, 1984, chap. 1.
[18] J. Wei, E. Iglesia, J. Catal. 224 (2004) 370.
[19] K. Sato, K. Nagaoka, H. Nishiguchi, Y. Takita, Int. J. Hydrogen Energy 34 (2009) 333.
[20] F. Gökaliler, B.A. Göçmen, A.E. Aksoylu, Int. J. Hydrogen Energy 33 (2008) 4358.
[21] X. Nie, E.I. Meletis, J.C. Jiang, A. Leyland, A.L. Yerokhin, A. Matthews, Surf. Coat. Technol. 149 (2002) 245.
[22] J.-W. Park, M. Kang, Int. J. Hydrogen Energy 32 (2007) 4840.
[23] K.H. Ang, I. Alexandrou, N.D. Mathur, G.A.J. Amaratunga, S. Haq, Ins. Phys. Publ. Nanotechnol. 15 (2004) 520.
[24] T. Panczyk, W. Gac, M. Panczyk, T. Borowiecki, W. Rudzinski, Langmuir 22 (2006) 6613.
[25] G. Du, S. Lim, Y. Yang, C. Wang, L. Pfefferle, G.L. Haller, J. Catal. 249 (2007) 370.
[26] H. Hirano, K.-I. Tanaka, J. Catal. 133 (1992) 461.
[27] L. Ma, D.L. Trimm, C. Jiang, Appl. Catal. A 138 (1996) 275.
[28] F. Sago, S. Fukuda, K. Sato, K. Nagaoka, H. Nishiguchi, Y. Takita, Int. J. Hydrogen Energy 34 (2009) 8046.
[29] J.G. Seo, M.H. Youn, I.K. Song, Int. J. Hydrogen Energy 34 (2009) 1809.
[30] V. Mazzieri, F. Coloma-Pascual, A. Arcoya, P.C. L'Argentie're, N.S. Fígoli, Appl. Surf. Sci. 210 (2003) 222.
[31] M. Shao, L. Kong, B. Hu, G. Yu, Y. Qian, Inorg. Chem. Commun. 6 (2003) 555.
[32] N. Laosiripojana, S. Assabumrungrat, J. Power Sources 158 (2006) 1348.
[33] P.K. Cheekatamarla, C.M. Finnerty, J. Power Sources 160 (2006) 490.
[34] K. Takehira, T. Shishido, P. Wang, T. Kosaka, K. Takaki, J. Catal. 221 (2004) 43.
[35] K. Nagaoka, K. Sato, H. Nishiguchi, Y. Takita, Catal. Commun. 8 (2007) 1807.